European Organization for Nuclear Research
CERN AB Departement

CERN-AB-2007-004
CARE-Report-06-033-HIPPI

The CERN SPL Chopper Structure: A Status Report

T. Kroyer, F. Caspers, E. Mahner

Abstract

In the framework of HIPPI, a study for a Superconducting Proton Linac is being carried out at CERN. An integral part of the medium energy line is the chopper, which has to establish the required time structure of the beam by cutting out selected bunches from the continuous bunch train coming out of the RFQ. Due to the bunch spacing of 2.84 ns a system rise and fall time of 2 ns is required. A slow wave structure matched to the beam speed of $0.08c$ was chosen as the most promising candidate. This structure was implemented as a meander line printed on a ceramic substrate. The mechanical design as well as technological issues are discussed. Furthermore, the results of comprehensive tests on the prototype are reported.

Geneva, Switzerland
October 2006

Contents

Chapter 1

Introduction

In the low energy section of the current Superconducting Proton Linac (SPL) design a fast chopper is foreseen after the RF quadrupole for establishing the required micro pulse-structure of the beam. This chopper is a travelling-wave kicker that deflects unwanted bunches to the beam dump. Due to the bunch bunch spacing of 2.84 ns the rise time should be below 2 ns to avoid partly chopped bunches. The chopper comes in two identical units in series, each in a 50 cm long tank where 40 cm long deflecting plates are installed. The most demanding mode of chopper operation will be when the SPL acts as injector into a ring machine, when it needs to remove three out of eight bunches in up to 0.6 ms long bursts with a repetition rate of 50 Hz. The SPL layout is illustrated in Fig. 1.1.
Due to the slow beam velocity of $\beta = 8\%$ up to six bunches will be on the chopper plates at the same time. Therefore the plates have to be operated in travelling-wave mode. A meander-like slow-wave structure that matches the speed of the electromagnetic wave to the beam is printed on the plates. This report discusses in particular the design, manufacturing technology and testing of the chopper plates as well as the overall integration of the chopper plates into the vacuum tanks.

1.1 The CERN chopping scheme

The chopping will be done at a proton energy of 3 MeV, which has been chosen as a compromise between beam dynamics considerations and the chopper amplifier. At lower energies a large emittance growth would result from the relatively long drift space

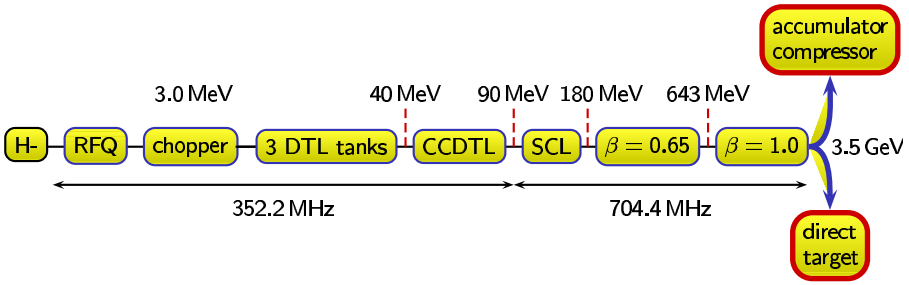

Figure 1.1: Schematic layout of the SPL (courtesy: F. Gerigk).

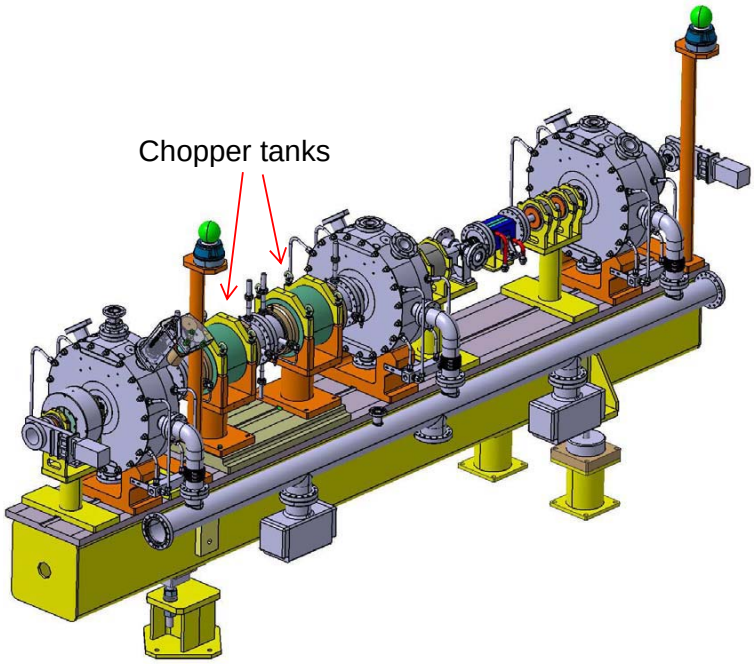

Figure 1.2: Integration of the chopper line.

housing the chopper, while higher energy would make the amplifier requirements more demanding. In order to reduce the drive voltage the chopper the lattice was optimized such that the kick is amplified by a downstream quadruple [1]. In this scheme it is foreseen to fit the chopper into existing quadrupoles which allows to reduce the length of drift spaces and avoid too abrupt phase changes in the lattice, which is important for limiting space-charge induced emittance growth. The nominal value of the effective voltage on each plate is 400 V, but due to the fact the a real structure has always less kick field than an ideal device with two infinitely extended planes (coverage factor < 1), somewhat higher voltages of the order of 600 V will have to be applied. The distance between the two plates is 20 mm. The plates are going to be driven at opposite polarities, which gives at total effective voltage of 800 V or the required kick field of 40 kV/m. A deflection of 5.3 mrad will be obtained for this kick.

Fitting the chopper into existing quadrupoles introduces additional constraints. The two 50 cm long chopper tanks will sit inside the 25 cm long quadrupoles. That leaves a length of about 40 cm for each pair of deflecting plates; the aperture of the tank is 95 mm.

The chopper line is shown in Fig. 1.2. In addition to the chopper and its beam dump it houses three buncher cavities and beam diagnostics. In the front and back section the matching from the RFQ and to the DTL are done.

The most demanding SPL scenario for the chopper is “neutrino operation” as injector into an accumulator and compressor ring. Pulses of 0.57 ms length with an average current of $I_{pulse} = 70$ mA are produced at the RFQ output at a 50 Hz repetition rate. The chopper then removes three out of eight bunches, leaving a pulse current of ≈ 40 mA. This scheme is illustrated in Fig. 1.3.

A beam dynamics simulation of the chopper line is shown in Fig. 1.4. The two choppers

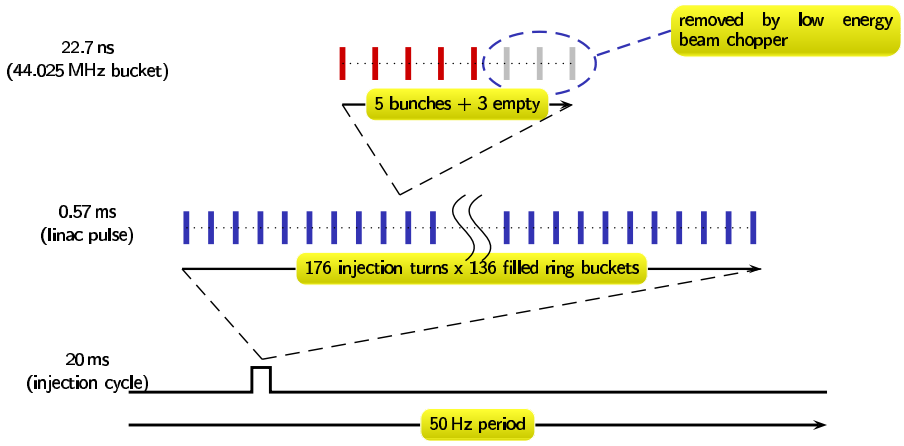

Figure 1.3: The timing scheme for "neutrino operation", the most demanding scenario for the chopper (courtesy: F. Gerigk).

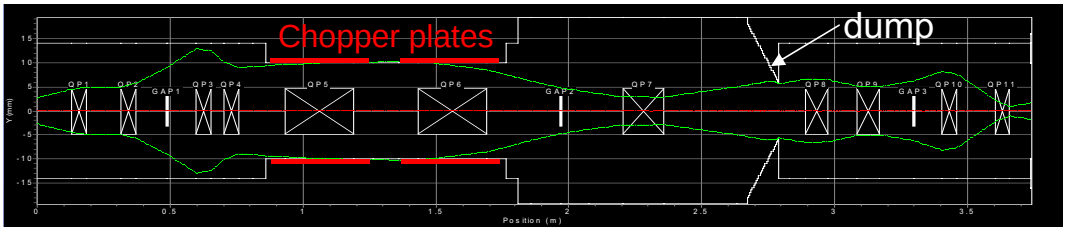

Figure 1.4: Beam dynamics simulation of the chopper line. The vertical 5 rms beam size containing 93% of the particles is plotted in green (courtesy: E. Sargsyan).

make a vertical kick and are installed in two vertically focussing quadrupoles. The beam size reaches its maximum in the space between the two chopper tanks, however, the beam envelope also touches the chopper plates and beam losses of the order of 1% are possible. Therefore the chopper plates must be able to stand the radiation as well as the beam loss related heating. Tens of Watts of dissipated power are expected for SPL operation, which must not lead to excessive heating. Therefore the thermal resistance between the chopper plates and the tank or some other heat sink should be sufficiently low and water cooling is required.

Chapter 2

Design

Since the bunch spacing is much shorter than the plate length up to six bunches will be on the chopper plates at the same time. Therefore, in order to avoid partially chopped bunches, the chopper must be designed as a travelling-wave structure matched to the speed of the beam. There is a number of requirements on the chopper that will be detailed in the next section.

2.1 Desirable chopper features

The chopper has to fulfill tough electrical specifications, in particular the short rise time. In addition it has to stand a significant amount of radiation and therefore a considerable heat load. It must operate in ultra-high vacuum and have sufficient high voltage capabilities. The new design should meet as many of these requirements as possible.

2.1.1 Electrical parameters

There is a number of electrical requirements the chopper should fulfill. Ideally it should have a very short rise time, low attenuation and provide almost as much kick field as a full two-plate line (high coverage factor). In addition it should be able to stand pulses in the kV range. In this section the requirements for the individual parameters are quantified as a basis for the practical design, which will have to find a compromise between these often conflicting demands.

RF parameters

The chopper is going to be designed as a travelling-wave device matched to the speed of the beam. The main RF parameters and their impact on the chopper performance are discussed now.

Transmission attenuation. Depending on the technology used the pulse propagating along the chopper plate may suffer a significant attenuation. This leads to a kick field reduction in the back of the chopper plate. For a characterisation of the whole plate the kick field has to be integrated over the length. The line attenuation will therefore be averaged over the plate length.

$\Delta E/E$ [%]	$\bar{A}$ [dB]
1	0.087
3	0.26
5	0.45
10	0.92

Table 2.1: Averaged transmission attenuation $\bar{A}$ as a function of the allowed kick field reduction $\Delta E/E$.

Let's assume an attenuation A in dB at the end of the plate, averaged over the relevant frequency range. After averaging over the plate length we get for the average attenuation $\bar{A} = A/2$ (always in dB). The relation between $\bar{A}$ and the averaged kick field reduction $\Delta E/E$ is given by

$$\bar{A} = 20 \cdot \log_{10}(1 - \Delta E/E)[\text{ dB}] \tag{2.1}$$

This equation is evaluated for a few $\Delta E/E$ in the Table 2.1. The equivalent average impedance can be calculated using the lumped element impedance formula [13]

$$Z = -2Z_0 \ln(1 - \Delta E/E) \tag{2.2}$$

where Z_0 is the line impedance. However it has to be noted that using the above definition (average over the relevant frequency range) both $\bar{A}$ and Z give the losses shortly after a rising pulse flank, i.e. it applies to the first chopped bunch. At later times the losses on the plate will decrease and tend towards the one given by the relatively low DC resistance.

Electrical length. In the chopper line the H^- beam has a kinetic energy of $E_{kin} = 3.019$ MeV. The rest mass of the H^- ion is $E_0 = 939.294$ MeV. Therefore we get a relativistic γ of

$$\gamma = \frac{E_0 + E_{kin}}{E_0} = 1.0032141 \tag{2.3}$$

and subsequently a beam velocity $\beta = v/c$

$$\beta = \sqrt{1 - \frac{1}{\gamma^2}} = 0.079984 \tag{2.4}$$

For a slow-wave line having a length of $L = 40.0$ cm the required electric length (delay) is

$$\tau = \frac{L}{\beta c} = 16.68 \text{ ns}. \tag{2.5}$$

An error in the line's electrical length causes the pulse on the plate to run at a different speed as the beam. Therefore the rising and/or falling edge of the kick pulse may cut into an adjacent unchopped bunch. Since the electric length of the plate is very long compared to the rise time budget (≈ 17 ns versus 2 ns), the relative error on the electric length must be very small. Errors below 0.1 ns, corresponding to less than 0.6% should be aimed for.

Rise time. The 2.84 ns bunch spacing is given by the RFQ frequency of 352.2 MHz. Assuming a maximum bunch phase length of $\pm 45^\circ$ the bunch length is 0.71 ns, which leaves 2.13 ns for the chopper rise- and fall time. The remaining kick field for the unchopped beam should be below 2%. The values commonly quoted are 2.0 ns for the 10 to 90% rise time and 2.5 ns for both the 3 to 90% rise time and the 90 to 3% fall time [1, 23, 25].
As a first approximation when dispersion is neglected, the rise times of the individual systems can be added up quadratically. The pulse generator together with the transmission lines will probably need most of the rise time budget. For the chopper structure itself the goal should be to add as few as possible to the overall system rise time. The system rise time at time t when running along the plate follows from the generator and structure rise times t_G and $t_S(t)$ as

$$t_r(t) = \sqrt{t_G^2 + t_s^2(t)} \tag{2.6}$$

The structure rise time $t_s(t)$ increases linearly from zero at the beginning of the structure to t_S at the end, where it can be quantified by measurement. The averaged system rise time is then approximately given by

$$t_R^2 = \frac{1}{t_S}\int_0^{t_S} t_r^2(t)dt = \frac{1}{t_S}\int_0^{t_S} (t_G^2 + t^2)dt = t_G^2 + t_S^2/3 \tag{2.7}$$

A 20% contribution from the chopper plates appears to be a reasonable goal, yielding $t_S = 2.08$ ns for a $t_R = 2.0$ ns.

Match. A travelling wave from the pulse generator will run along the chopper plates. It is important to have a good match between the 50 Ω transmission line coming from the generator to the travelling-wave structure. The potential problems from possible mismatches are twofold.

- Power loss due to reflection. In terms of S-parameters, a given reflection S_{11} reduces the amplitude of the transmitted wave S_{21} and therefore the kick field by $\sqrt{1 - |S_{11}|^2}$. This reduction should be smaller than 1% and negligible ideally.
- Reflected power from the end of the slow-wave structure may give an unwanted kick to unchopped bunches. This kick should be lower than 2% of the full kick strength. A impedance mismatch between the 50 Ω feed line and the slow-wave structure will give rise to the voltage pulse being reflected and running back on the plate as a pulse of similar time structure. A localised discontinuity on the other hand, e.g. from connectors will act differently, since it will only cause two short reflected peaks of opposite polarity. For short discontinuities their length is comparable to the structure rise time of roughly ≈ 1 ns. The impact of these two peaks should almost cancel and their interaction with the beam will be limited due to the small transit time factor of the order of 1 ns/(2 · 17 ns) ≈ 0.03.

Fig. 2.1 shows both quantities as a function of S_{11}. In order to get negligible kick field reductions S_{11} should be smaller than about -20 dB. As for the line impedance of the slow-wave structure, matching to better than -30 dB is necessary in worst case conditions. If the kick pulse is at least twice as long as the chopper plate (≈ 34 ns)

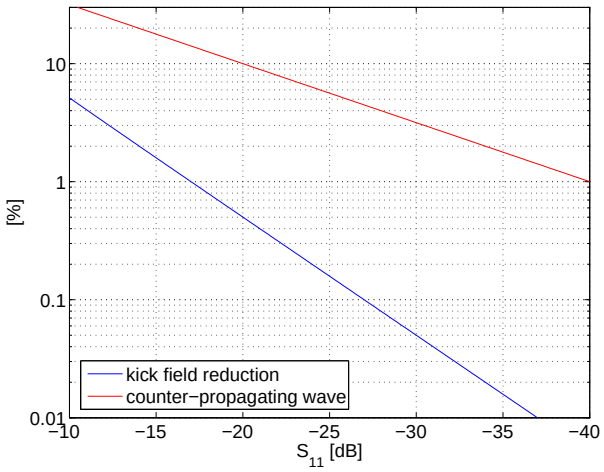

Figure 2.1: Kick field reduction and magnitude of wave reflected from the end of the slow-wave structure as a function of the matching.

the first unchopped bunch would see an unwanted kick field almost all along the plate. For the following bunches and/or shorter pulses the effect is smaller. As an example, for "neutrino operation", where three out of eight bunches are removed, an unchopped bunch would see a spurious kick field over roughly 3/8 of the line. A matching to $S_{11} < -30$ dB sets the limits for the line impedance as $Z_L = 50 \pm 3\ \Omega$.
An isolated discontinuity on the other hand will have a much lower impact. For isolated reflections below -20 dB no significant unwanted kick is expected.

Coverage factor

The coverage factor (CF) is defined as the ratio of the obtained kick field to the field for an ideal structure with infinitely extended full-metal plates at the beam position. Obviously the CF should be as high as possible, since any reduction will entail an increase in the required voltage. Values of about CF = 0.8 appears as a realistic target. In addition to achieving a certain value on the beam axis the CF should be homogeneous over the beam aperture. However, since the chopper should only *remove* certain bunches, a higher than average kick field is not a big problem; it may just lead to losses before the beam dump. A too low kick field results in residual chopped beam which should be avoided as far a possible, since it may lead to problems further down the linac. As the beam dump is round [4], it may be possible to have a lower off-center kick field. This would somewhat ease the specification on the kick field homogeneity. Beam dynamic simulations including a nonhomogeneous kick field are currently being performed.

High voltage

For a nominal kick field of 40 kV/m and a CF of 0.8 a plate voltage of $U = \pm 500$ V to ground is required. For smaller and/or not homogeneous CFs a somewhat larger $U \approx 600$ V may be required. Therefore the structure must be able to stand pulses of > 600 V to ground for each plate and > 1200 V between the two plates. For the rather large plate distance of 20 mm the Kilpatrick limit at 10 MHz is beyond 100 kV [6].

Potential high voltage limitations should therefore only be encountered between the individual plates and ground.

2.1.2 Radiation and heat

In the most demanding SPL mode for "neutrino operation" 0.57 ms pulses with an average current of $I_{pulse} = 70$ mA are produced at the RFQ output at 50 Hz repetition rate. Continuous beam losses on the chopper of $\lambda = 1\%$ are possible on the chopper plates [1]. The chopper plates must be capable of standing both the radiation and the induced heat load.
The duty factor for "neutrino operation" is $\delta = 0.57$ ms/20 ms $= 2.85\%$. Since the beam is intercepted at a kinetic energy of $E_{kin} = 3$ MeV most of the beam energy is actually converted into heat in the "target" material.

Heat load. The average power deposited by the beam on all four plates is then

$$P_b = I_{pulse}/e \cdot E_{kin}[\text{eV}] \cdot e \cdot \lambda \cdot \delta = 34 \text{ W}. \tag{2.8}$$

Electrical losses of the pulsed power supply will add to the heat load. Assuming a stationary state with a DC voltage U on the chopper, the Ohmic losses are given by

$$P_{DC} = \left(U \cdot \frac{R}{R_0 + R} \right)^2 \frac{1}{R} \tag{2.9}$$

where R designates the DC chopper resistance and R_0 the system impedance. For typical values of $U = 600$ V, $R = 1\ \Omega$ and $R_0 = 50\ \Omega$ we get stationary losses of $P_{DC} = 140$ W for one single plate. However, since the electrical duty factors are low, in the worst case about $3/8 \cdot \delta \approx 1\%$, the Ohmic losses should be of the order of 1.5 W per plate or $P_{el} = 6$ W for all four, which is far less than expected from radiation.
The total power $P = P_b + P_{el} = 40$ W will in fact come in 50 Hz pulses of $P/50$ Hz $=$ 0.8 J. The thermal contact to the heat sink must be good enough and/or the thermal capacity of the chopper plates must be large enough not to heat too much during each pulse.
For the metals considered for the deflecting structure, such as silver or copper, the resistivity temperature coefficient is roughly $\alpha = 4 \cdot 10^{-3}$ K^{-1} [2]. A temperature increase of 100 K then leads to a 40% resistivity rise, corresponding to a 20% increase in RF losses, which should be tolerable. The thermal resistance R_{th} between *all four* chopper plates and their respective heat sinks should be below 100 K/40 W $= 2.5$ K/W. For *one* chopper plate we then have $R_{th} < 10$ K/W for equally distributed losses.

Radiation resistance. Protons impacting on a target at $E_{kin} = 3$ MeV lose their energy mostly by electronic excitation, ionization and elastic scattering. Inelastic reactions are only possible by tunnelling and therefore very rare. In the nickel-coated chopper beam dump the protons are absorbed in the first ≈ 100 μm of the material [4, 5]. Since the mass number of Ni is very close to the one of Cu that will probably be used for the slow-wave structure, similar proton ranges are expected. Due to the grazing incidence the ranges could be even lower. Depending on the exact geometry

and thickness of the metallic line a substantial amount of radiation may still reach the underlying material.
A worst-case estimate of the radiation dose can be done starting from the deposited power. In Equation 2.8 a worst-case beam loss of roughly 34 W was found. Over one year of full SPL operation this integrates to 1 GJ. Assuming as a first approximation a homogeneous absorption in the top 50 μm of a 10 mm wide strip on the chopper plates the affected volume is $\approx 10^{-6}$ m^{-3}. For a density of metals like copper an excessive dose of $\approx 10^{11}$ Gy per year follows.
Damages to organic materials start to become significant between 10^3 Gy (Teflon) to 10^8 Gy (Epoxy resins, glass filled polyester) [5, 8]. For metals this dose should not pose much problems as long as the heat load can be handled [7]. Copper can be used above at least 10^{10} Gy and ceramics such as Al_2O_3 or MgO above 10^9 Gy [9]. However, for very high doses volume swelling may occur in ceramics, while a decrease in metal conductivity might be found. Material degradation due to sputtering could also be possible.

2.1.3 Vacuum requirements

The chopper tank is part of the chopper line vacuum system. Owing to the short time that the protons spend in the accelerator, the pressure requirements given by the lifetime considerations is 10^{-7} mbar as for the rest of the normal conducting linac section. Only in the source and the low energy beam transfer line vacuum requirements are lower (10^{-5} mbar). Due to very little space available pumping manifolds have been designed for the Chopper Line. The apertures (diameters) of the beam tube vary between 26 and 147 mm. Any material used in the chopper tanks must be ultrahigh vacuum compatible, cleaned and carefully assembled.
The whole linac pumping system must be compatible with the vacuum equipment typically used in CERN accelerators. The evacuation of the vacuum system from atmospheric pressure will be done with pumping groups (primary and turbo molecular pumps) and lumped sputter ion pumps, standard Penning/Pirani gauges will be distributed for pressure logging during operation. The whole vacuum system must be metal-sealed using either Conflat^{TM}(all vacuum equipment) or Helicoflex^{TM}seals (joints between tanks), O-rings are excluded. The vacuum control of all machine equipment has to be compatible with the existing CERN installations.

2.2 Existing structures

Two kinds of slow-wave structures are reported in literature:

- A line composed of metallic strips across the aperture and coaxial cables that connect each strip to the next one downstream. The electrical length of this line is tuned mainly by adjusting the length of the coaxial cables [21, 22, 11]. Rise times of the order of 1 ns can be obtained. Since the metallic strips in general cover a rather large fraction of the surface, the coverage factor of such structure is high (> 0.8). However, due to the long coaxial cables such structures are not easy to integrate in applications where space is limited. An implementation of such a structure within the HIPPI framework is reported in [10, 11].

- A meander line printed on a dielectric substrate [14, 15]. The matching of the wave velocity to the beam is done by adjusting the meander width for a given substrate permittivity ϵ. Such structures would also meet the present rise time requirements, however radiation resistance and heat transfer capability of the dielectric material have to be checked. An advantage of this kind of structure is that very compact designs should be possible and that the mechanical complexity is limited.

2.3 The CERN structure

Due to the given space constraints a meander line structure appeared to be the most promising candidate. When printed on a high permittivity substrate it is possible to reduce the transverse meander dimension and fit the chopper plates into the existing quadrupoles.

2.3.1 Choice of parameters

Three main parameters have to be determined for a meander line, namely the substrate, the shape of the line and the conductor material.

Substrate

A ceramic material was chosen for a number of reasons:

- good radiation resistance, in particular compared to organic materials
- good vacuum properties
- good heat resistance and conduction
- high ϵ implying small transverse meander size

However, a drawback is that printing on ceramics is a difficult procedure. Alumina (Al_2O_3, $\epsilon_r \approx 9.8$) was chosen since it is widely used in RF engineering and meets very well the above requirements.

Conductor

High purity silver or copper are the materials of choice for the conductor material. Due to the differential heat expansion between these metals and alumina and for crystal lattice matching an intermediate layer is necessary. The electrical conductivity of this layer will be considerably worse than of the main conductor. If it is thin compared to the skin depth not much current will flow there so it will not influence much the electrical properties.

Line geometry

The substrate thickness should be ≥ 3 mm for sufficient mechanical robustness. The electrical parameters were determined using formulas and graphs given in [16]. For larger substrate thickness the coupling between lines increases, which leads to more

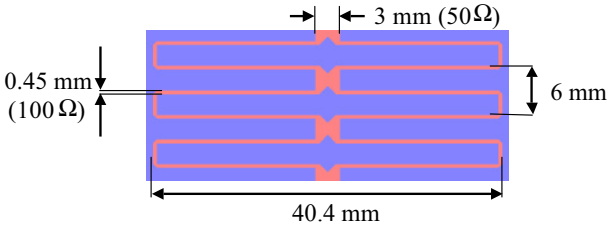

Figure 2.2: Geometry of the double meander line showing three elementary cells. The 50 Ω line is composed of two 100 Ω lines folded into meanders. The substrate is 3 mm thick alumina with $\epsilon_r \approx 9.8$. Starting from analytical results the exact dimensions were determined in numerical simulations.

dispersion. A thinner substrate on the other hand would cause higher Ohmic conductor losses. A ceramic thickness $h = 3$ mm was chosen as a compromise.
At first the parameters of a 50 Ω meander line were determined. However it turned out that the line width needs to be very close to the substrate height. In this case the spacing between parallel line would be small, leading to high dispersion. In addition there would be problems with the first transverse structure resonance, which occurs when the meander width equals a quarter wavelength in the dielectric.
These problems can be avoided by combining two 100 Ω lines to form one 50 Ω double meander (Fig. 2.2). Please note the wide conductor sections in the middle where we have a single 50 Ω line. Using [16] the effective permittivity for the 100 Ω line with $\epsilon = 9.8$ is evaluated to $\epsilon_{r,eff} = 5.9$, the line width is $w = 0.15h = 0.45$ mm.
Since the length of the structure is limited to 40 cm, the only free design parameter is basically the length of the elementary cell. As its length increases

- the coupling between adjacent lines and therefore dispersion decreases.
- the electrical length decreases, which has to be compensated by making the meander wider. That lowers to frequency of the transverse resonance. Since the dispersion increases as one approaches this resonance it should be well above the operational frequency range (0 to 200 MHz).
- the coverage factor decreases slowly and the electric field gets more inhomogeneous longitudinally.

A hard limit to the meander width is given by the aperture of the quadrupole. In a compromise between dispersion, transverse size and coverage factor a meander period a 3 mm was chosen. In this way the structure is wide enough to limit the coverage factor decay towards to sides, while the meander period is still much shorter than the beam aperture. In addition the dispersion should be acceptably low.
The meander width was determined from

$$\tau = \frac{L}{c/\sqrt{\epsilon_{r,eff}}} \tag{2.10}$$

where $\tau = 16.68$ ns designates the required electrical length and L the total length of the meander line. The obtained geometry was used as a starting point for 3D electromagnetic simulations using CST Microwave Studio to get the exact value for the

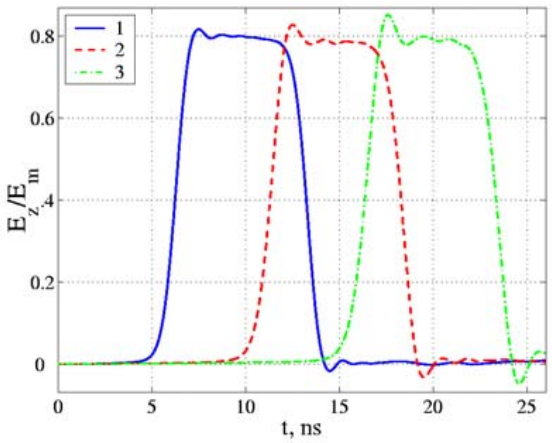

Figure 2.3: Time domain simulation results of the meander structure: The normalized on-axis kick pulse for a 2 ns rise time pulse after running along 12.5, 25 and 37.5 cm of the meander line.

meander width $m = 40.4$ mm. Fig. 2.2 shows the final dimensions. Since there is coupling between adjacent lines Equation 2.10 tends to overestimate the electrical length. 66 meander cells fit onto the 40.6 cm long plates, with a 5 mm straight line on either side for contacting the coaxial connector.
In the center of the structure where the two 100 Ω lines join, local impedance matching was done by triangular cuts (Fig. 2.2).

2.3.2 Simulations

Time domain simulations

Full 3D electromagnetic simulations with time domain excitation have been done under CST Microwave Studio to confirm the design and evaluate the dispersion and coverage factor. The results were in agreement with measurements, in particular the S-parameters, the pulse delay and the port impedance [12]. First noticeable resonances of the structure were found at 1.65 GHz. Fig. 2.3 shows the evolution of a pulse with 2 ns rise and fall time as it travels along the dispersive structure. The plotted deflecting electric field on the beam axis is normalized to the maximum field achievable in the same structure with a continuous metal surface, i.e. it represents the coverage factor. One can clearly see an overshoot that grows with distance, which is related to the dispersive meander line.

Electrostatic field simulation

Since the meander line covers only a small fraction of the ceramic surface it is clear that the field pattern will be considerably different from a band line. Assuming a continuous excitation of the meander line an electrostatic approach can be used to calculate the field pattern. However, close to the pulse fronts this method will not necessarily give valid results, since RF effects enter the game. There are several important points to be examined:

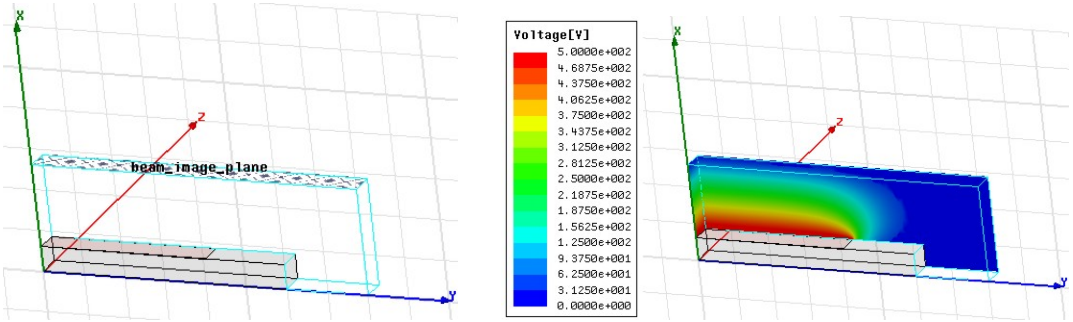

(a) Geometry used for the simulation. The right side of a ceramic plate was modelled, the beam axis is on the x-axis at the position of the "beam image plane".

(b) The potential when the conducting layer is set to 500 V over ground.

Figure 2.4: Electrostatic simulation of a reference line with a conductor covering the full surface of the meander line.

- Field strength on the beam axis with respect to what is expected for an infinitely extended conducting plane. This parameter is commonly referred to as coverage factor (CF).
- Field homogeneity, in particular of the vertical kick field seen by the particle, that is, integrated over the length of the structure.
- Fringe field leaking out at the structure and field reduction towards the plate ends

As the length of the structure is much longer than the vertical aperture (400 mm versus 20 mm), the latter effect is expected to be very small and will be neglected. To evaluate the first two effects, modeling an elementary meander cell is sufficient when the correct boundary conditions are applied. The simulations were run under Ansoft Maxwell.

Reference geometry. As a starting point, a fully metallized conductor as illustrated in Fig. 2.4(a) was used. Only a 3 mm long section of the right plate half was modeled. Magnetic boundaries (electric field tangential to plane) on the back and front side make the structure look infinitely extended along the x-axis. A magnetic boundary on the left side forces right-left symmetry and an electric boundary on the top (electric field normal to plane) models the second plate.
Fig. 2.4(b) shows the potential when the meander is excited with 500 V. The vertical electric field E_x is displayed in Fig. 2.5. On the right E_x is plotted as a function of transverse position. On the beam axis almost the same electric field strength as for an infinitely extended plane is found. On the right side of the structure 10 mm of vacuum were modeled before the metallic wall that represents the chopper tank.
In further simulations it was found that

- having a wider conductor does not increase the electric field in the center any more. The present geometry is just wide enough that E_x reaches its maximum in the center.
- Increasing the distance to the tank wall does not change much the field decay on

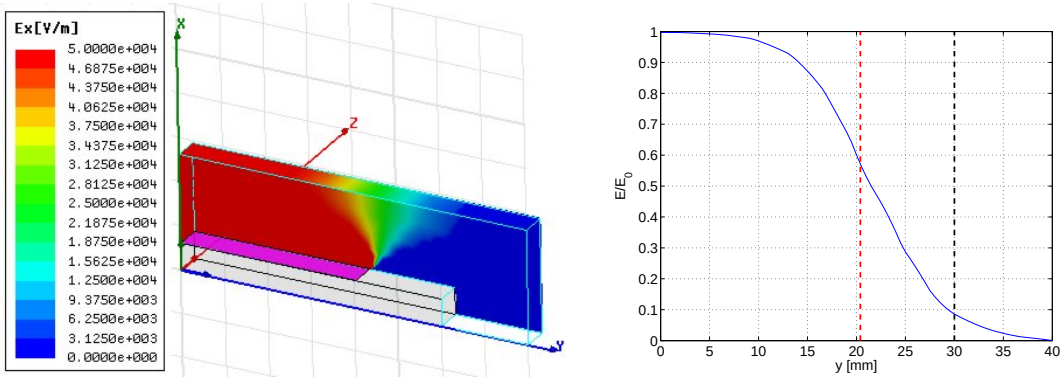

(a) Color plot of E_x.

(b) Horizontal cut of E_x at the beam position. The red dashed line indicates the edge of the conductor, the black line the edge of the dielectric.

Figure 2.5: Vertical electrical field E_x for the reference line.

the sides. Therefore the presence of the tank should not affect the kick field in the center of the structure.

Elementary cell of the meander line. In order to keep the structure as small as possible only the elementary cell consisting of half a meander on the right side of the lower plate was modeled (Fig. 2.6). The beam axis is in the upper left corner of the structure parallel to the z-axis. Magnetic boundaries on the front and back side then produce a periodic single meander line. Another magnetic boundary in the center makes a double meander out of it and an electric boundary on the top plane enforces the symmetry representing the second chopper plate with opposite polarity voltage. The parameters of the real structure were used as far as known. The exact line width and thickness may vary in dependance of the technology used; an estimated 0.5 mm width and 50 μm thickness were used. The permittivity of the alumina plate was assumed to be $\epsilon = 9.8$.
Fig. 2.6(b) shows the electric potential in the elementary cell. Close to the conductor surface rather large changes in potential can be seen which gradually average out as one comes closer to the beam axis. This is reflected by maxima in the vertical electrical field close to the conductors (Fig. 2.7(a), red regions). Between the conductors the electric field tends to bend down to the dielectric due to the high ϵ (blue regions). However, such small-scale variations of E_x average out in the total kick.
In this section the coverage factor $CF = E_x/E_0$ will be averaged over the cell length. Here $E_0 = 50$ kV/m is the maximum possible kick field for a 500 V over the 10 mm half aperture. The convergence of the simulation as a function of the mesh iteration is shown in Fig. 2.7(b). Interestingly enough, the CF appears to decrease monotonically when the meshing is improved, converging to 0.765 after 10 to 13 iterations.
The CF is not very sensitive on the exact value of ϵ, however it was found that a 10% increase in line width causes a 1.6% CF increase. Using a very thin line (surface current) the CF decreases by roughly 1%.

The field homogeneity over the aperture is illustrated in Fig. 2.8. The contour plot on the left depicts the normalized kick field averaged along the beam axis. This represents

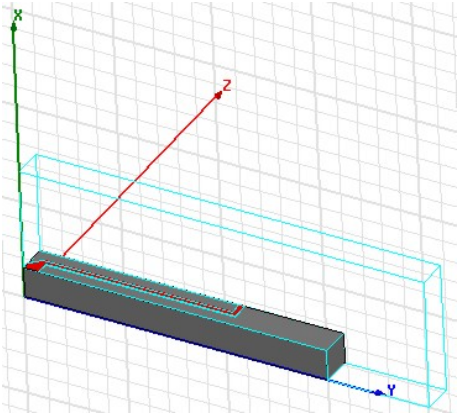

(a) A quarter-meander on one plate was modeled. Using the appropriate boundary conditions this structure can model a periodic two-plate meander line.

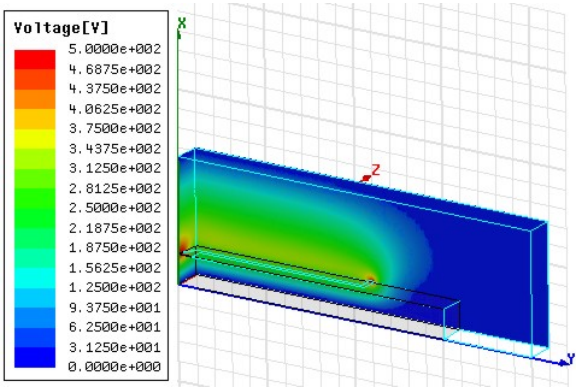

(b) Potential when the meander is set to 500 V.

Figure 2.6: Elementary cell of the meander line. The beam axis is at the upper left corner of the structure

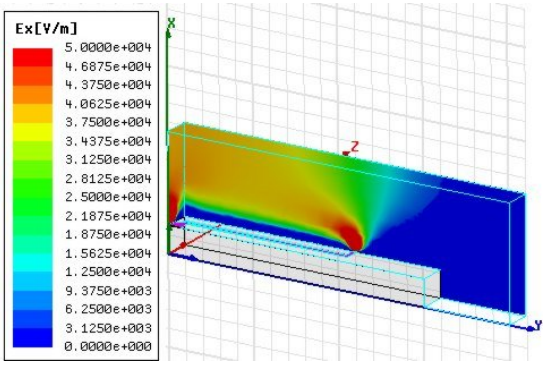

(a) Close to the conductors E_x has maximum values, while it can also be negative between them (blue regions).

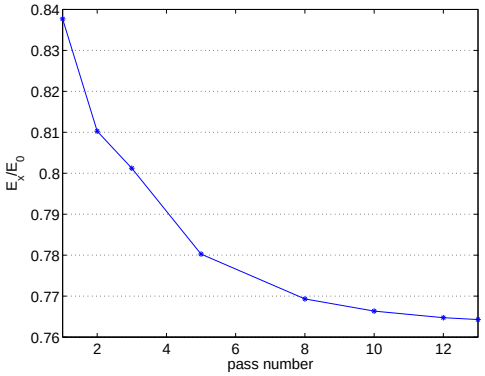

(b) Convergence of the normalized on-axis electric field (CF).

Figure 2.7: Vertical electric field on the meander line.

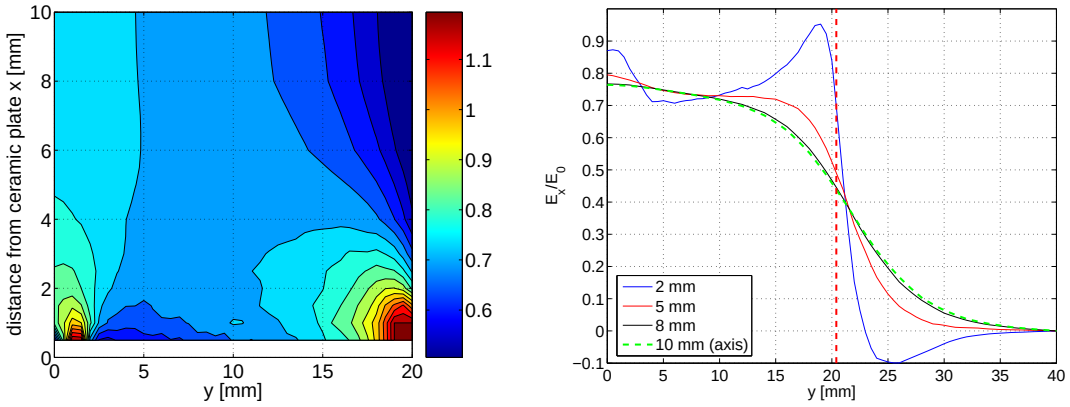

(a) Contour plot of the averaged kick field E_x/E_0 in the chopper aperture. The beam center is in the upper left corner ($x = 10$, $y = 0$ mm)

(b) Transverse cuts through the contour plot at different distances x from the plate. As x gets larger the E_x gets more homogeneous.

Figure 2.8: E_x averaged along the beam axis. Close to the largest conductor surfaces in the center and at the side maxima are found with a shallow minimum in between. On-axis the coverage factor reaches a value of 0.76. The extremity of the meander line at $y = 20.4$ mm is indicated as a red dashed line.

the CF as a function of position. On the right transverse cuts at several distances from the plate surface are shown. As was already seen before the kick field is larger close to the conductors, while it gets more and more homogeneous when approaching the beam axis. About $y = 5$ mm to the side of the beam axis and very close to the ceramics E_x is smaller than on-axis on account of the electric field bending back down to the dielectric. This effect is very pronounced to the right of the meander line ($y \geq 20.4$ mm). When getting closer to the center of the structure the transition region around $y = 20$ mm gets smoother and more field "leaks out" to the side.
A plausibility check can be done by verifying Gauss' law

$$\mathbf{\Phi} = \oint_S \mathbf{E} \cdot d\mathbf{A} = \frac{1}{\varepsilon_o} \int_V \rho dV \tag{2.11}$$

with the electric flux $\mathbf{\Phi}$, the electric field $\mathbf{E}$, the differential surface area $d\mathbf{A}$ and the space charge density ρ in the volume V. Considering the meander line as an infinitely extended line charge, the electric flux through all closed surfaces around it is constant. Let's use two horizontal planes as this closed surface, one going through the dielectric below the meander line and one above in the air. In this case we have to integrate over E_x. As E_x decreases fast for large y we can neglect the contribution at large enough y. Now it follows from Gauss' law that for the upper plane $\int E_x dA = const$ for all vertical positions $x > 0$. In Fig. 2.8 the longitudinal average which is proportional to the integral is plotted. Therefore the transverse integral over y has to be constant for all $x > 0$. This was verified to be the case to a precision better than 1%. Fig. 2.8(b) illustrates very well that when going from the plate towards the beam axis the field that was initially concentrated close to the conductors "pours out" into the space on the side.

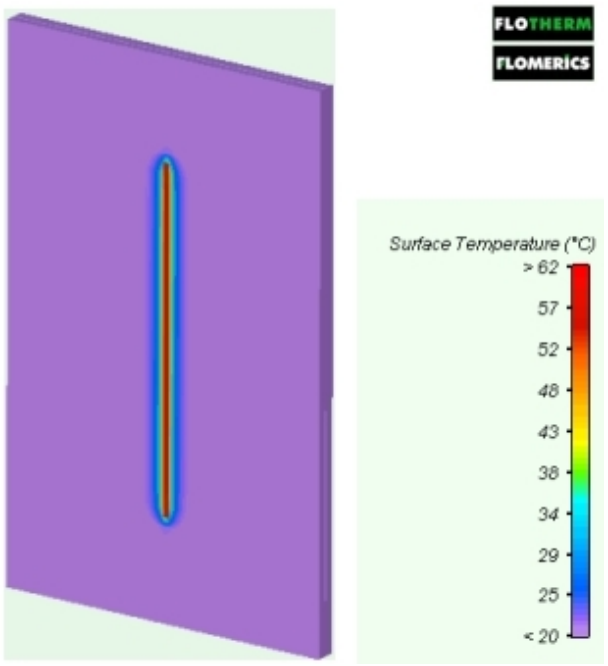

Figure 2.9: Simulation of the heat transfer from a printed line to the ceramic substrate (courtesy: Flomerics Ltd.).

Heat conduction

The heat transfer from the meander line to the ceramic substrate was investigated in a numerical simulation using the Flotherm code [18]. A 100 mm long straight section on cooled ceramic plate as shown in Fig. 2.9 was simulated. Since copper is a very good heat conductor the most significant part of the thermal resistance stems from the metal-ceramics junction. A model benchmarked with measurements for FR4 epoxy-bound glass fibre circuit boards was used. This model should also be applicable to ceramic substrates [17]. For a 1 mm wide and 100 mm long conductor a thermal resistance $R_{th} = 0.66$ K/W was found. Scaling to the meander line of full length ≈ 6000 mm and width ≈ 0.5 mm we get an $R_{th} \approx 0.02$ K/W between the meander line and the ceramic plate was found.

Assuming worst-case losses with a $P = 10$ W heat load per plate the copper will be

$$\Delta T = PR_{th} = 0.2 \text{ K} \tag{2.12}$$

hotter than the ceramic plate. The heat capacity of the copper line on one plate is $C \approx 0.5$ J/K. During one 0.57 ms pulse 0.2 J are deposited on one plate. Neglecting heat conduction during that short time a temperature rise of

$$\Delta T = P/C = 0.4 \text{ K} \tag{2.13}$$

is expected during each pulse. In both cases the temperature excursion is low.

Summary

Simulations to determine the coverage factor of the meander line structure were carried out. An excellent agreement with discrepancies in the 1% range was found using differ-

ent simulation tools. In the electrostatic simulation using Ansoft Maxwell a $CF = 0.764$ on the beam axis was found. At 10 mm horizontal offset the CF decreases to 0.717. Slightly larger values were found in an electrostatic simulation by Gayther with CST EM Studio, namely $CF = 0.778$ on axis and $CF = 0.729$ for a 10 mm horizontal offset [10]. In [12] results from electrostatic simulations under MAFIA and time domain electromagnetic simulations under CST Microwave Studio were reported, predicting a CF = 0.79 on the beam axis. In a heat transfer simulation is was found that the conductor excess temperature should be of the order of 1 K.

2.3.3 Electromagnetic compatibility

The 2 ns rise time chopper pulses will have spectrum with a 3 dB point at about 200 MHz. However, significant spectral components can be expected well above, up to 500 or even 1000 MHz. Due to a number of beam diagnostics systems close to the chopper tank, special attention has to be paid to electromagnetic compatibility issues, in particular wrt. waveguide mode propagation in the beam pipe. Due to the specific design of the pulser no problems are expected there. In case something problem are still encountered, additional shielding can be installed [24].
The connecting high voltage cables should be sufficiently RF tight. To prevent signal leakage screw-lock connectors are used throughout the design. As for the chopper itself, signal leakage through waveguide modes in the beam pipe is possible. The beam pipe diameter at the upstream and downstream side of the chopper are 25.1 and 40 mm, respectively. In the larger downstream beam pipe waveguide cut-off is at 4.4 GHz, which is more than a factor 20 above the driver's 3 dB point. The spectral components in this frequency range should be very small and therefore waveguide modes should not present a problem, either.

Chapter 3

Implementation

3.1 Ceramic plates

The procedures used for the making microwave integrated circuits (MIC) can be used to create the meander line on the ceramic substrate. There are three basic metallization techniques:

- Electrochemical deposition allows to make rather thick purity layers. However, it can only applied on a suitable metallic base material.
- By thin film technology very thin layers can be made using vacuum deposition. High material purity and therefore good conductivity can be obtained. However, the required thicknesses for reaching low DC resistance are hard to reach. In addition to that the layer adhesion on ceramics is not very strong, which may lead to mechanical problems.
- Thick film technology does not give very pure conductors, but it provides very good bonding to the ceramic surface. Typical layer thicknesses are around 10 to 15 μm after firing. Electrochemical deposition of copper or silver can then be used to decrease the line resistance.

It was decided not to metallise the back side of the ceramic plate but rather attach it mechanically to a solid metallic ground plane. This way a high ground plane conductivity is readily obtained. In addition it would not be easy to make a well-defined contact between a metallized ground plane and the support structure. This choice implies however that gap of a few μm will remain between the ceramic and the ground plane, whose impact on vacuum and heat conduction must be checked experimentally. The electric field will be enhanced in the gap. From the conservation of electrical flux it follows that the ratio $E_{gap}/E_{dielectric}$ equals the dielectric's ϵ_r. For a typical 600 V plate voltage we get $E_{gap} \approx 2MV/m$ which should not lead to problems in vacuum.

3.1.1 Prototyping at CERN

Thick film technology appeared most suited for our application and was therefore used for the prototype production at CERN. The ceramic plates were procured from Wesgo in Erlangen, Germany. In several iterations the technological parameters were optimized.

First prototype. A 19.2 cm long double meander with 10 to 15 μm thick film paste was produced as first prototype. A number of technological rules had to be observed. In order to keep the thermal stress in the alumina within reasonable limits heating/cooling rate should not exceed 50 to 100° C per hour. It is mandatory to do the firing in air to allow the formation of metal oxides. This requires the selection of thick film paints which can endure long exposition to air at high temperatures. Secondly, the paint on the fired substrate must stand the aggressive acids during chemical etching. Certain conductor paints, which are good for extended heat exposure are dissolved by these acids and thus cannot be used.
Evaluating the structure it was found that the silver paint does not reach the bulk conductivity; a high DC resistance of slightly more than 10 Ω over 50 cm was found. This showed that it is necessary to add another layer with electrochemical deposition.

MoMn matching layer added. A 12 to 20 μm MoMn thick film layer was used instead of the silver, since MoMn very well matches the alumina crystal lattice and provides high bonding strength. Then 20 to 30 μm of silver layer were added electrochemically as the main conduction layer. The DC resistance of this structure decreased about eightfold to 1.3 Ω over 50 cm. However the layer bond to the MoMn turned out to be very bad.

Final procedure. By adding an intermediate layer between the MoMn and the Ag a satisfying results were found. The final layer structure is depicted in Fig. 3.1(a). The procedure works as follows:

- The ceramic plate is supplied from Wesgo with one side covered by a homogeneous MoMn layer. During its production the MoMn paste is fired at 1500° C in a H_2/N_2 atmosphere with a resulting layer thickness between 12 and 20 μm. The ceramic material used here is AL300 with a purity of 97.6% and 1.6 μm surface roughness. The processing at CERN starts with sputter etching to clean the surface during two minutes with a DC power of 50 W in an argon atmosphere of 10^{-1} mbar.

- The plate is then coated with two different layers by magnetron sputtering. The coating system is equipped with two planar magnetron sources of 150 mm diameter. After 24 hours of pumping and a bake-out at 150° C a pressure of $5 \cdot 10^{-9}$ mbar was obtained.
  To increase the adherence of the silver layer, an intermediate layer of 0.5 μm titanium is deposited at an argon pressure of $1.1 \cdot 10^{-3}$ mbar. Earlier tests with sputter etching only and with titanium but without sputter etching did not give good adherence. Sputter etching needs to start with a clean surface and the titanium is necessary for its good crystallographic compatibility with MoMn. Directly sputtering silver onto the MoMn results in poor adherence despite all surface cleaning efforts.

- A layer of 2 μm silver is then deposited on top with the same argon pressure. During these two coating runs the plate is moved in front of the sources several times in order to obtain a uniform coating thickness.

- Finally the thickness of this silver layer is increased up to 30 μm by electrochemical deposition.

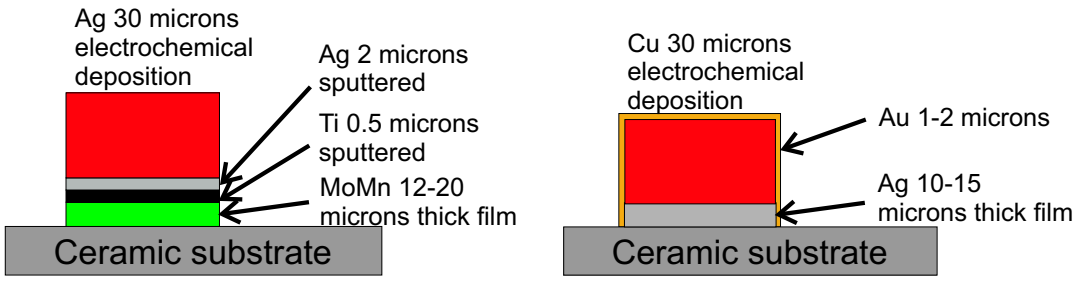

(a) The method developed at CERN is rather complex. Three intermediate layers were needed before deposition of the main conductor.

(b) A more straightforward process involving only three layers was used by Kyocera.

Figure 3.1: Comparison of the printing technologies used for the meander line.

- The ceramic plate is now homogeneously coated. A subsequent chemical etching with the customary photo resist technique creates the desired meander pattern. However, the presence of three different metals coatings requires three different chemical baths.

In RF tests this plate performed very well. However the fabrication procedure is complex and rather costly. All process parameters must be very controlled to insure a good repeatability of the results. For these reason it was decided to go to industry for the "series" production.

3.1.2 Production in industry

In a cooperation with Kyocera the manufacturing process was reviewed and adapted to the available technology. The alumina plates are produced in-house. After a few iterations a more direct way to implement the meander structure was found. Fig. 3.1(b) shows the obtained layer structure. First a 10 to 15 μm silver thick film layer is applied. This provides less bonding strength to the ceramic than MoMn but is still sufficient. The 30 μm copper main conduction layer can then be deposited electrochemically. Finally a thin finishing of gold is applied for low contact resistance and as a protection against oxidation.

3.2 Mechanical implementation

The main difficulty for the mechanical implementation was to fit the structure into the tank with 95 mm inner diameter while keeping the installation procedure simple and clean. In order to provide good mechanical stability for the ceramic plate a 10 mm thick, 70 mm wide and 46 cm long aluminum plate was used as ground plane (Fig. 3.2). The RF connection to the meander line is done with a feedthrough through a hole in the ground plane. An feedthrough with ceramic dielectric procured from the company PMB was used [19]. Then the signal is guided in a straight vertical coaxial line without dielectric to a second feedthrough at the top or bottom of the tank. At this point we have the transition from the tank vacuum to the outside world. A Conflat^{TM}feedthrough (DN 16 CF) with N type connector from Caburn was used [20]. During assembly the inner conductor of the line is plugged onto the center pin of the feedthroughs. The

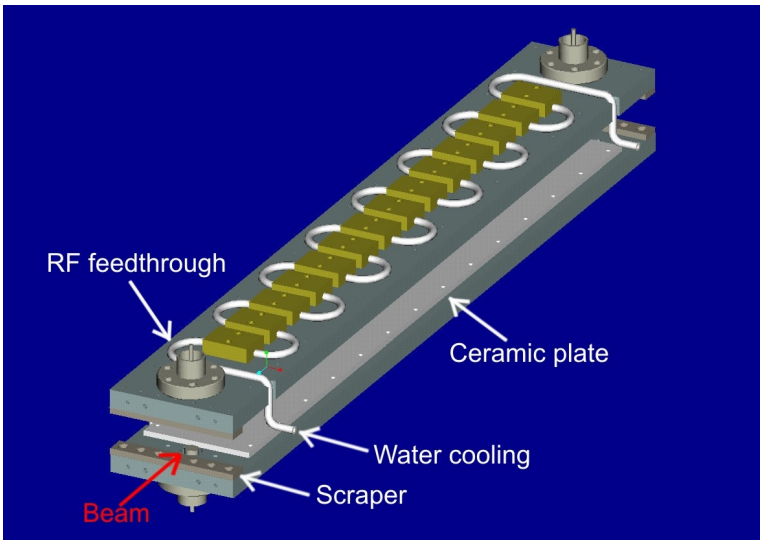

Figure 3.2: Two two ceramic plates fixed on their support plates with the water cooling lines mounted on the back.

transition from the coaxial line to the meander is done with a short copper band line. On the back of the ground plane the water cooling is installed. Special care has to be taken to ensure leak tightness since the cooling circuit operates in the tank vacuum. On front side a small copper "scraper" is placed that protrudes by ≈ 0.3 mm farther into the beam aperture than the ceramic plate to limit beam losses there. This should be effective in particular for the second chopper tank where the beam envelope has its maximum size close to the beginning of the plate (Fig. 1.4). For the first tank and for chopped beam, however, the scraper is not expected to reduce much the losses on the ceramic plates.

Fig. 3.3 shows both chopper plates installed in the tank inside the quadrupole (green). RF and water lines come out on the top and bottom and on the sides, respectively. DC breaks for the triaxial chopper structure as foreseen in initial plans are shown. However, the concept of DC-wise floating plates was given up and the DC breaks left out in the actual prototype assembly. The ground plates are held in place by two support rings at the ends of the tank. Each of these rings can be aligned with three screws. This way the position of the plates can be easily adjusted. It is also possible e.g. to tilt them to change the kick strength or to reduce beam losses on the ceramic plates. Finally, tank after installation of the first plate is shown in Fig. 3.4.

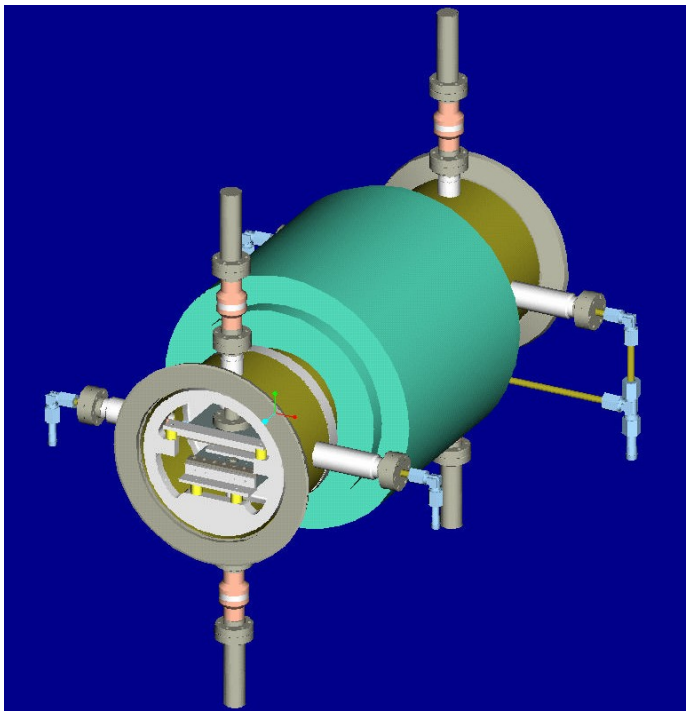

Figure 3.3: The fully installed chopper tank inside the quadrupole. The RF lines are on the top and bottom, the water cooling on the sides.

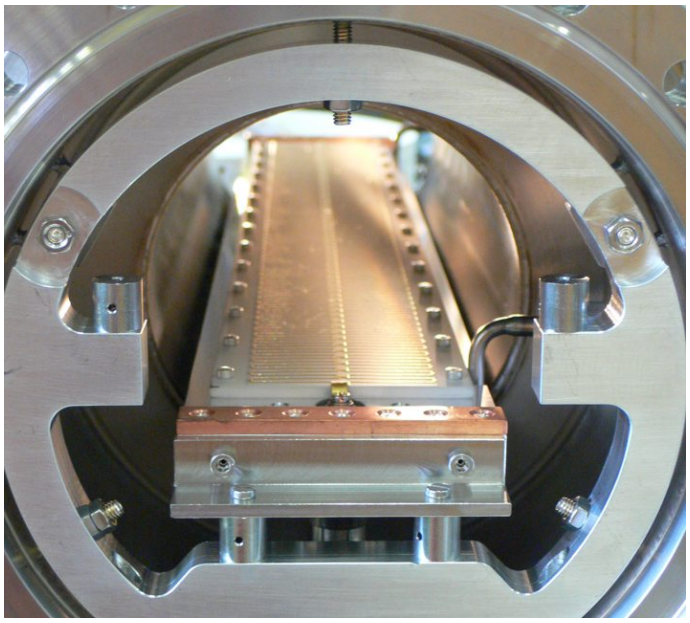

Figure 3.4: The first plate installed in the chopper tank. The copper scraper can be seen in the front. Behind it in the center is the RF connection to the meander line. On the right the water cooling is connected.

Chapter 4

Prototype testing

In August 2006 the second ceramic plate was delivered by Kyocera. After having found very satisfactory results in the RF tests on the single plate it was installed in the tank. The results of comprehensive tests, including vacuum, leak tightness, heat transfer and high voltage are reported in this chapter.
Fig. 4.1 shows the set-up for the prototype testing. The single ceramic plate is installed at the position of the lower plate and connected to water cooling circuits (right side) and the RF feedthroughs at the beginning and end of the meander line.

4.1 RF properties

A series of RF measurements were performed on the chopper plate before and after its installation in the tank. Since the chopper is going to be pulsed with $t_r \approx 2$ ns rise time (10 to 90%), we expect a spectrum starting to roll off at $1/(3t_r) = 170$ MHz (3 dB point). We will refer to the frequency range between 0 and 200 MHz as *operational frequency range*. Since significant spectral components are expected up to 500 MHz and above, most measurements were done up to 1 GHz.
For a full RF characterization of the chopper plate three main criteria have to be evaluated:

- The electric field strength on the beam axis integrated over the chopper length. For this parameter the transmission attenuation ($|S_{21}|$) as well as the reflection (match, S_{11}) in particular at the beginning of the line have to be determined. The transmission attenuation has to be averaged over the length of the structure to find its effect on the effective kick field. Reflections at the end of the line will cause undesired waves running back on the structure that can kick unchopped bunches.

- The group velocity of the wave on the meander line. This parameter can be extracted from the phase of S_{21}. It must be noted the a possible error in electrical length cannot be "averaged" over the length of the plate, since it will in any case cause to chopper to cut into the back of the previous unchopped bunch or into the beginning of the next unchopped bunch.

- The rise time t_r. Mainly the phase distortion and the attenuation, both given by S_{21}, contribute to the finite rise time of the meander line. The total chopper rise

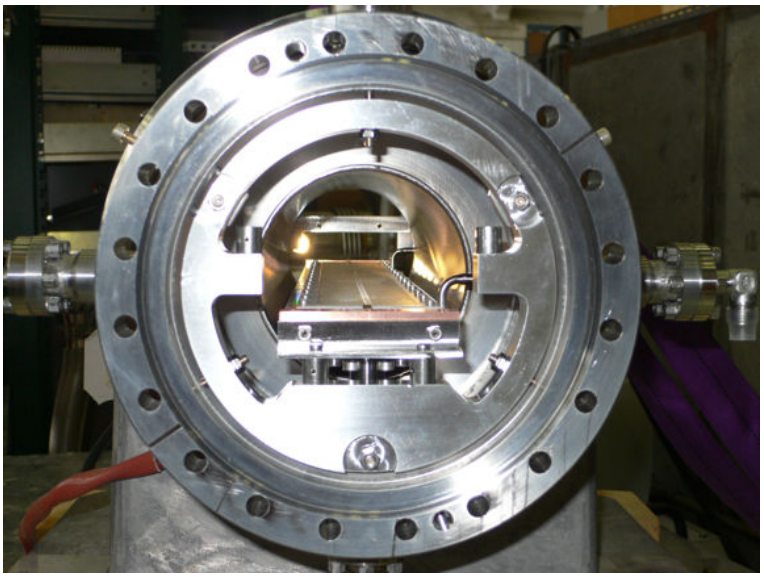

Figure 4.1: The chopper tank with a single ceramic plate installed for testing.

time should not exceed 2 ns. In order to calculate the effective rise time as seen by the beam, an average has to be taken over the length of the plate.

To put it in a nutshell, it is necessary to determine the full S matrix of the chopper plate. All measurements were done using a full two port calibration. After a series of measurements on the single chopper plate it was installed in the tank and the measurements repeated. Since except for a slight increase in reflection no significant changes were found, mostly the single plate data will be presented. In order to enforce the two-plate symmetry during operation, for the characterization of the single chopper plate a horizontal metal plate was placed at the position of the beam. By the use of this "image plane" the electric field at the beam axis will be strictly vertical like under operational conditions.

4.1.1 Transmission attenuation

The transmission magnitude S_{21} of the single chopper plate is shown in Fig. 4.2. This attenuation was measured at the end of the plate. In order to get the effective electrical field along the line, averaging over the operational frequency range and over the plate length has to be done. The frequency domain averaging yields about 0.6 dB attenuation at the end of the line. After spacial averaging we the get 0.3 dB of effective attenuation, corresponding to a kick field decrease of 3.4%. At DC a resistance of 1.1 Ω was measured, in line with the low frequency limit of S_{21}. At 1.62 GHz the first meander line resonance was found.

4.1.2 Electrical length

The *electrical length* of the chopper plate is the time a wave takes to run along the meander line. Of course this quantity will depend on frequency, which gives rise to

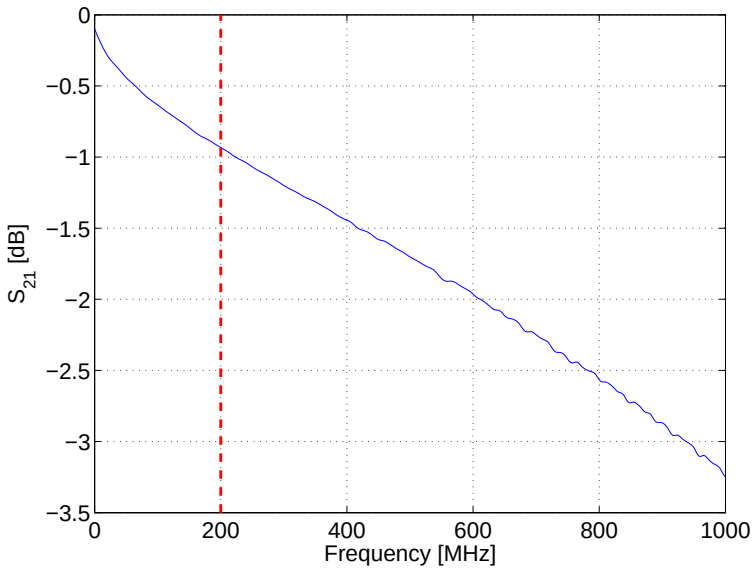

Figure 4.2: Magnitude of the transmission over the full length of the chopper plate. The limit of the operational frequency range is indicated by the dashed red line. Due to attenuation a kick field decrease of $\approx 3\%$ is expected.

dispersion. In practise the electrical length can be determined either by exciting the structure with a suitable pulse or step and measuring the delay or from the slope of the phase of S_{21} as a function of frequency. Fig. 4.3 shows the phase of S_{21}, from which the electrical length was calculated. Without image plane the electrical delay is 16.73 ns, with image plane the curves are very similar qualitatively but a slightly larger electrical delay of 16.83 ns was found, which is within 0.1 ns of the required length.
Comparing Figs. 4.2 and 4.3(a) it can be seen that the -3 dB point is at much higher frequency than the $-45°$ phase point (940 vs. 375 MHz, respectively). Compared to an idea low pass [3] the high dispersion stands out, indicating that the rise time will be limited by dispersion rather than by attenuation. This dispersion is due to coupling between parallel line sections and increases fast with frequency. Below 20 MHz the electrical length increases slightly a result of the skin effect in the layered conductor structure. At low frequencies the current is distributed over the entire conductor surface while it is concentrated on the lower side of the well-conducting copper layer at high frequencies. This gives rise to an increase in line inductivity at low frequencies, which in turn decreases the group velocity, an effect similar to the low-frequency properties of coaxial lines [28].

4.1.3 Rise time

For the determination of the meander line rise time the driver pulse was approximated by an appropriate function. The step function depicted in Fig. 4.4(b) has the required $t_{in} = 1.97 \approx 2$ ns rise time. A Kaiser Bessel function with 500 MHz bandwidth and a parameter $\beta = 6$ was used. The spectrum of such a pulse is shown in Fig. 4.4(a).
At the output of the meander line a slightly longer pulse with $t_{out} = 2.21$ ns is observed.

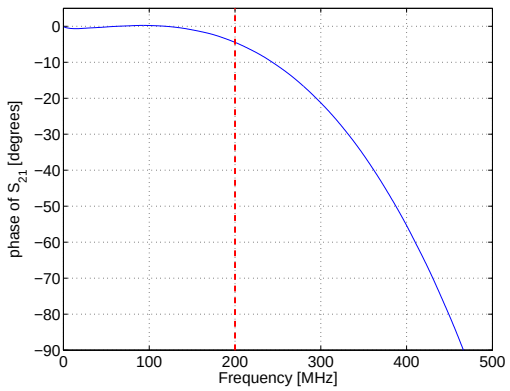

(a) Phase of S_{21} with the 16.73 ns of electrical delay removed. Above 200 MHz the phase distortion grows fast.

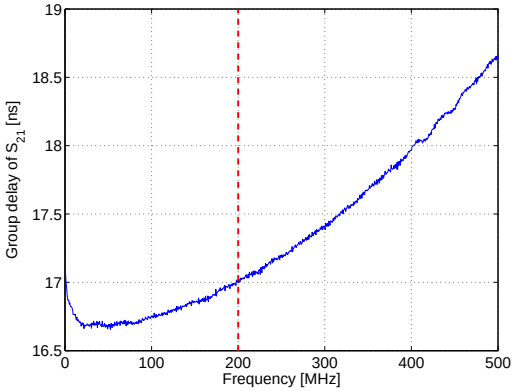

(b) The group delay varies between 16.68 and 17.00 ns in the operational frequency range.

Figure 4.3: Determination of the electrical length of the meander line without image plane.

The rise time of the meander structure can then be estimated as

$$t_S = \sqrt{t_{out}^2 - t_{in}^2} = 1.00 \text{ ns}. \tag{4.1}$$

The averaged system rise time for this input pulse is evaluated to $t_R = 2.08$ ns according to Equation 2.7. When much shorter input pulses are used larger t_S are found since the plate is operated in the highly dispersive region of the plate response. The minimum rise time reached for very short input pulses ($t_{in} = 0.11$ ns) is $t_{out} = 1.37$ ns. However, for a realistic $t_{in} > 1.4$ ns $t_S < 1.05$ ns, which is a very satisfying result. For too long input pulses on the other hand t_S appears to grow, which is probably due to the limited validity of Equation 4.1.

4.1.4 Match

In order the check the match between the 50 Ω feed line and the meander line the reflection coefficient S_{11} was measured in frequency and time domain. The results from measurements on the single plate are shown in Fig. 4.5. A very good match with $S_{11} < -30$ dB was found below 500 MHz. The time domain step response is plotted in Fig. 4.5(b). It gives the reflection coefficient at a given position on the line, thus allowing to verify the homogeneity of the line. In contrast to an ideal transmission line, due to losses S_{11} does not come back to the base line at the end of the meander line ($t \approx 37$ ns). Since $|S_{11}| < 0.02$ the line impedance is within ±2 Ω of the nominal 50 Ω.
After installation of the meander line in the tank the match was not as good as before. Probably the discontinuities stem from the transition between the coaxial line inside the chopper tank and the meander line. However, an average S_{11} of −25 dB over the operational frequency range is still acceptable. It may cause a very insignificant kick field reduction of $1 - \sqrt{1 - 10^{-25/10}} \approx 0.2\%$ and a short counterpropagating pulse of

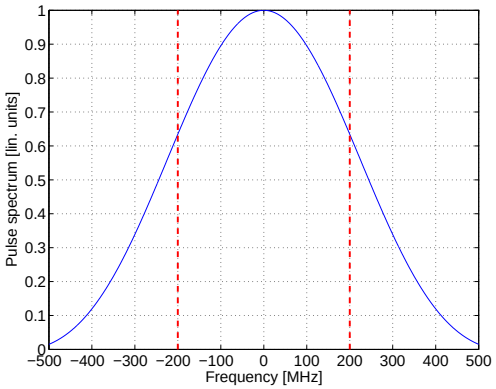

(a) Spectrum of the input pulse. A Kaiser Bessel function with $\beta = 6$ and ± 500 MHz bandwidth was used.

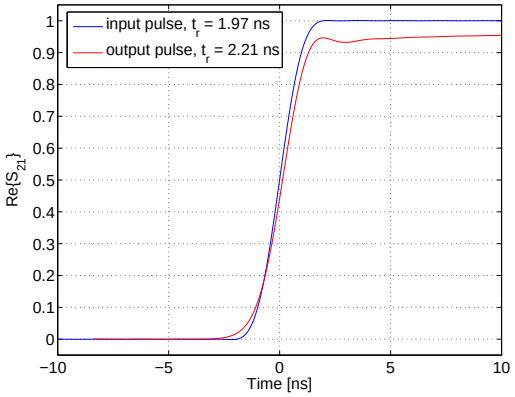

(b) Input versus output pulse on the chopper plate, yielding the meander line rise time of 1.0 ns.

Figure 4.4: Determination of the meander line rise time. The single plate installed in the tank was excited with a realistic step function modelling a pulse from the generator.

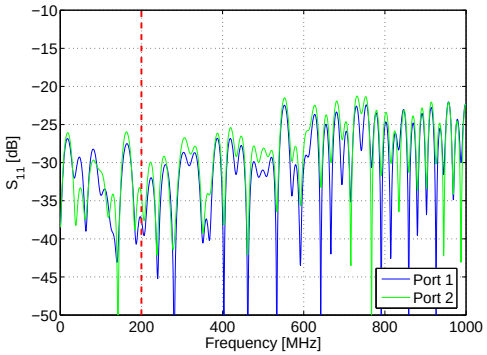

(a) Frequency domain: $S_{11} < -30$ dB averaged over the operational frequency range.

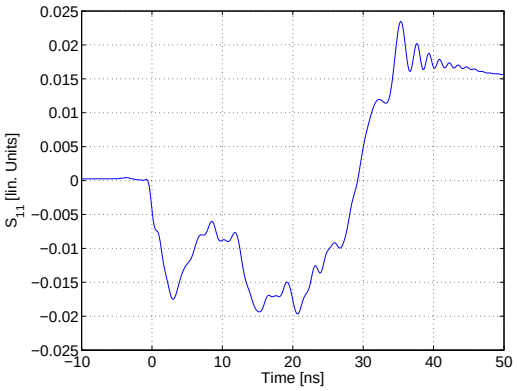

(b) Time domain: From the real part of the S_{11} step response the line impedance as a function of the position can be calculated. The match is better than $\pm 2\ \Omega$.

Figure 4.5: S_{11} measurements on the single plate without image plane.

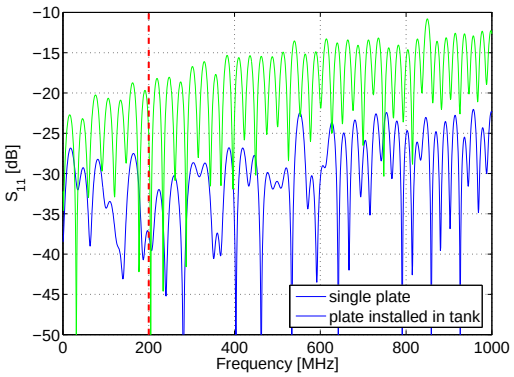

(a) Frequency domain: After installation the match deteriorated somewhat, which is probably due to discontinuities at the ends of the coaxial line inside the chopper tank.

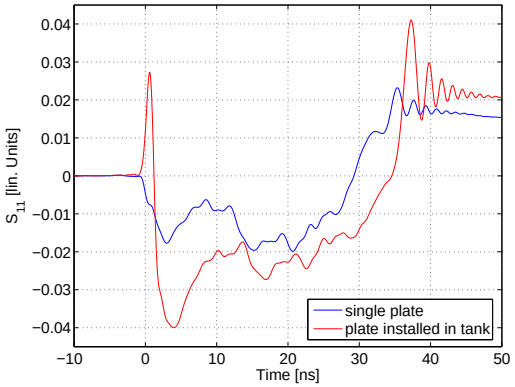

(b) Time domain: Distinct peaks can be seen at the beginning and end of the line, where discontinuities are suspected.

Figure 4.6: S_{11} measurements on the single plate installed in the chopper tank.

$10^{-25/20} \approx 6\%$ nominal field. Due to to bad transit time factor this isolated discontinuity should not pose problems.

4.1.5 Sensitivity to presence of the image plane

The present structure proved to be very insensitive the the presence of the image plane. In other words, the properties do not change much when only one chopper plate is driven. For a single plate, when the image plane is added

- the electrical length *increases* by $\approx 0.5\%$
- the line impedance *decreases* by $\approx 1.0\%$
- the attenuation increases slightly, with a change of the order of 1% below 200 MHz.
- there is no significant impact on the rise time.

4.1.6 Tuning of electrical length

The electrical length of the meander line is a very important parameter. A significant deviation from the required value means that the chopper will cut into the bunch before and/or following these that should be kicked out. Since this parameter is not easy to control technologically it was tried to adjust it without changing the ceramic plate itself. This is possible by adapting the metallic ground plane. For a proof of principle two longitudinal grooves with a width of 5 mm and a depth of 3 mm were milled into the ground plane. This method has the big advantage that the rather fragile and costly ceramic does not need to be modified. However, the electrical length can only be decreased this way. The impact the grooves on the electric length is illustrated in Fig. 4.7.

The impact on the main RF characteristics can be summarized as follows:

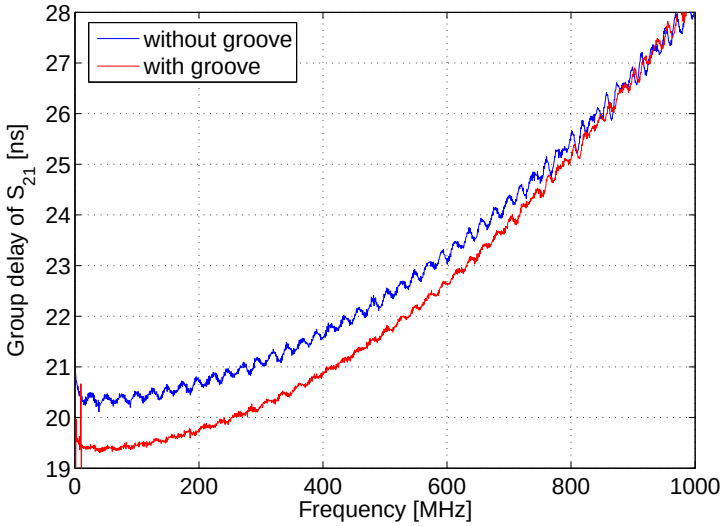

Figure 4.7: By cutting two 5 mm wide and 3 mm deep grooves into the metallic ground plane the electric length was decreased by 5%.

- the electrical length decreases by $\approx 5\%$
- the line impedance increases by $\approx 4\%$
- the attenuation below 200 MHz decreases by $\approx 6\%$
- there is no effect on the rise time ($< 0.02\%$).

Contrary to first intuition the groove does not cause large reflections, since the introduced discontinuities are rather small and below 1 GHz the distance between them is much smaller than the wavelength. Therefore they just change the line impedance. By chance, in the present case the match even become a bit better. The effect of the groove on the electrical length is about as large as on the line impedance and attenuation. However, since the requirements on electrical length are much more demanding, it can be adjusted without having a relevant impact on the other parameters.

4.2 Coverage factor

As an experimental check for the coverage factor (CF) simulation results presented in section 2.3.2, a measurement was performed on the meander line. The set-up is depicted in Fig. 4.8. A single ceramic plate with an metallic image plane at the beam position was used. In the center of the image plane a 10 mm wide button-type probe measures the electric field at and around the beam position. In order to calibrate the measurement in addition to the meander line as device under test (DUT) a reference line consisting of a fully metal-coated plate was used (REF, center in Fig. 4.8). In both cases we have a three-port device, with the input and output of the plate as ports 1 and 2 and the probe as port 3. The S-parameters of this structure at low frequency were measured for extrapolation to DC and determination of the CF.

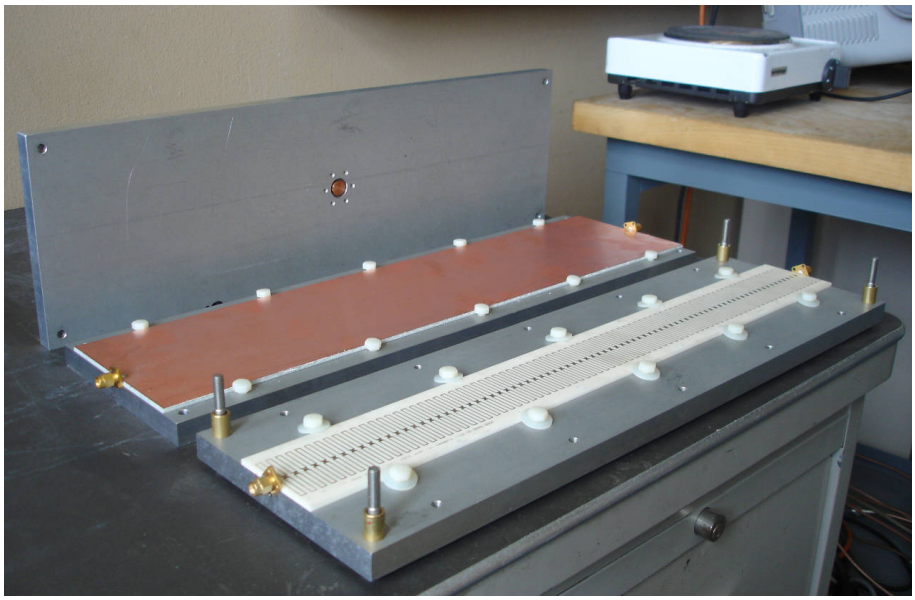

Figure 4.8: Set-up for the coverage factor measurement. The field on the beam axis is measured using a probe (top plate) for a reference line (center) and the meander line (bottom).

The measured quantities were S_{21} and S_{31} for both the REF and DUT, with the end of the line terminated with a matched load. Since the reference line is not matched to 50 Ω as the DUT, a strong mismatch was encountered which reduced the power coupled into the reference line. However, since this effect is present in both $S_{21,REF}$ and $S_{31,REF}$, it can be compensated. The data was evaluated under the following assumptions:

- The losses on the reference line are negligible, since its conductor cross-section is very large
- The mismatch of the DUT is small, but it has significant losses.

The CF can then be calculated as

$$CF = S_{31,DUT} - S_{21,DUT}/2 - (S_{31,REF} - S_{21,REF}) \text{ dB}, \tag{4.2}$$

where the S parameter have to be plugged in dB. The result is shown in Fig. 4.9 together with the maximum mechanical uncertainty, giving $CF = 0.78 \pm 2\%$. The approach used is only valid at very low frequencies, while residual mismatch of the meander structure and other effects may lead to unphysical results at higher frequencies.
A slightly different technique using an open circuit instead of the matched load at port 2 should give the same result, provided that Equation 4.2 is modified accordingly. $S_{21,REF}$ $S_{21,REF}$ is expected to double but the other S parameters should not be affected. The result of this cross-check at 1 MHz is plotted as a black star in Fig. 4.9, giving $CF = 0.81$. The measurement results obtained with both methods agree very well with the numerical simulations discussed before.

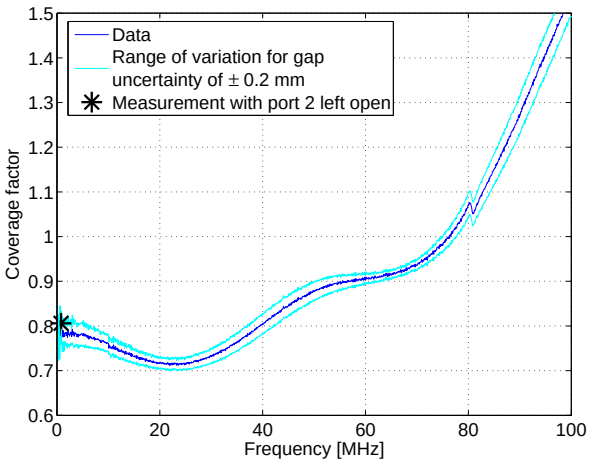

Figure 4.9: Measurement of the coverage factor. The applied method is valid only at very low frequencies, where $CF \approx 0.78$ was found.

4.3 Vacuum and leak test

The chopper tank with one ceramic plate installed (Fig. 4.1) passed the helium leak test successfully with a leak rate smaller than $2 \cdot 10^{-10}$ mbar·l/s, which corresponded to the background signal of the used leak detector.
There have been concerns that the air at the large ceramic plate – metal junction could act as a trapped volume leading to very long pumping times and "bad" vacuum. At first small problems were encountered with a limit pressure of $1.5 \cdot 10^{-7}$ mbar. However, this was probably due to a contamination of the ceramic plate or outgassing of the metal coating. The ceramic plate had not been baked under vacuum before installation, which is foreseen for future installations to prevent such problems. Electric heating of the chopper plate with the cooling off turned out to be a practical solution, since it provided a kind of "in-situ bake-out" of the ceramic plate. As can be seen in Fig. 4.10 the pressure rose by a factor 5 when heating the ceramic plate by 130 K above ambient temperature. After a few hours of "mild" baking a pressure of $3.5 \cdot 10^{-8}$ mbar was obtained, which is well within specifications ($1 \cdot 10^{-7}$ mbar) for the chopper line vacuum system [1].

4.4 Heat transfer

The ceramic plate carrying the meander line does not have a very well-defined thermal contact to the cooled metal support plate. It is attached to this ground plane with 28 silver-plated M2 steel screws which are only mildly fastened in order to allow the ceramic plate to move as a result of differential thermal contraction. There should be direct contact between the two plates only in a some points. In such a case the thermal contact resistance cannot be easily estimated and the method of choice is therefore an experimental measurement [26]. Due to the surface smoothness of the order of 1 μm relatively good thermal contact should be possible, as experience with AA stochastic cooling has shown [27].

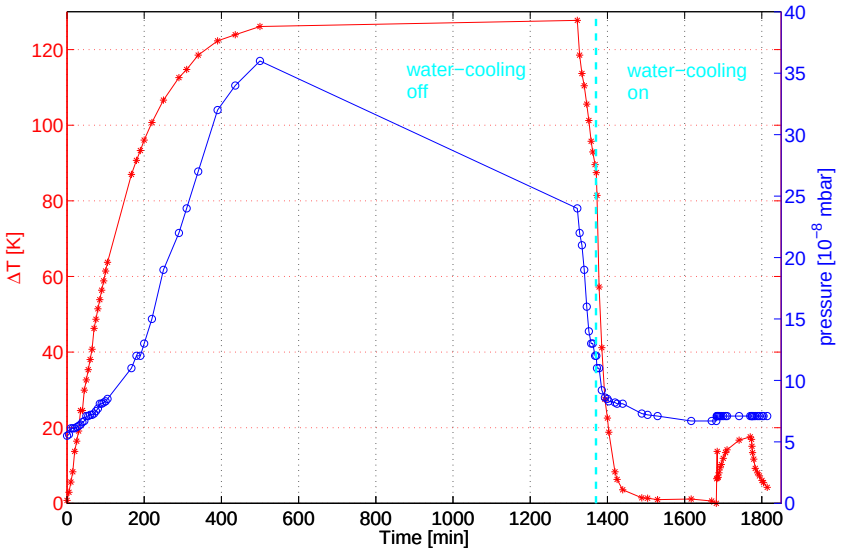

Figure 4.10: Heat test under vacuum on the single plate installed in the chopper. For a heat load of about 25 W a temperature increase of < 20 K was found with cooling on.

In order to settle the question about how much heat power can be dissipated in the chopper plates, a heat test transfer was carried out on the single plate installed in the tank. The meander line was driven with a 4 A current which caused resistive losses of about 25 W heating the meander line and the underlying ceramic plate. The voltage as well as the vacuum pressure were logged. The temperature coefficient of the resistivity for the conductor materials copper, silver and gold is $\alpha = 4 \cdot 10^{-3}$ K^{-1} [2]. The temperature increase ΔT can be calculated knowing the resistance at ambient temperature R_0 and the increased resistance R using

$$R = R_0(1 + \alpha \Delta T). \tag{4.3}$$

The temperature of the chopper plate was monitored with an infrared camera. This also allowed to examine the geometry of the heated surface and to detect possible hot spots. For evaluation of the data an emissivity of 0.9 was assumed for the alumina. Since the emissivity of the gold coated meander should be low we could expect to see mostly the radiation of the alumina there. However, due to the angular dependence of the emissivity the temperature readings would be strongly influenced by the exact view angle. Therefore the front face of the alumina was chosen as a reference point and the camera was positioned such that it was seen almost perpendicularly.

Fig. 4.10 shows the two heating cycles performed on the chopper tank. At first run heating was applied for more than 1300 minutes without water cooling. In the steady state $\Delta T = 128$ K was found with a heating power of 28.4 W, yielding a thermal resistance $R_{th} = 4.5$ K/W.
In this steady state heating was switched off at $t = 1300$ min and the beginning of the cool-down recorded. An exponential decay as expected for heat conduction was found. This indicates that other heat transfer mechanisms, in particular radiation, play only a

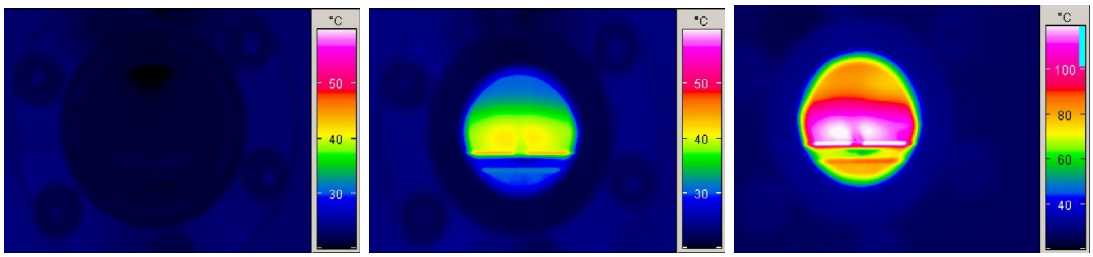

(a) $t = 0$ min, $\Delta T = 0$ K. (b) $t = 35$ min, $\Delta T = 20$ K. (c) $t = 500$ min, $\Delta T = 120$ K.

Figure 4.11: Observation of the plate's temperature profile with an infrared camera during the heat transfer test. Please note the change in scale in the rightmost picture.

minor role. An estimation of the maximum power radiated off a perfectly emitting plate surface gives powers of the order of 50 W. However the shiny metal surface on the inside of the tank limits heat transfer by reflecting back most of the incident power. When two chopper plates are installed, heat radiation from one plate will be intercepted mostly by the second plate, thus reducing still more the heat transfer to the tank. Therefore radiation should be negligible as heat transport mechanism in the present case.

The ΔT calculated from resistance was compared to direct readings from the infrared camera, showing very good agreement. Pictures taken during the first heating cycle are shown in Fig. 4.11. The highest temperature readings were found on the front face of the ceramic plate, where the emissivity is highest. No particular hot spots were detected.

Exponentials were fitted to the rising and falling edges to extract the heat transfer parameters under the assumption of a single thermal resistance linking the heated body to the heat sink. The fit quality was very good, indicating that this simple model should be valid. A heat capacity of about 2000 J/K was found which is much bigger then the one of the ceramic plate alone. It rather corresponds to the entire metal ground plate together with the support rings. These rings are connected to the tank by three steel screws (see Fig. 4.1) whose thermal resistance is apparently much bigger than the one of the ceramic-metal surface.

After about one hour the cooling circuit was switched on (light blue vertical marker in Fig. 4.10 until ambient temperature was reached. Then another heating and cooling cycle was carried out with the cooling on to keep the metal ground plane at room temperature. A much lower steady state $\Delta T = 18.2$ K was found for 20.4 W heat power, yielding $R_{th} = 0.89$ K/W. This is the thermal contact resistance between the ceramic and the ground plane under operational conditions. Since a stand-alone cooling circuit was used, the coolant flux was limited and the ground plane temperature might have increased somewhat. The thermal resistance quoted above should thus be a pessimistic estimate.

To summarize, it was found that the thermal resistance between the ceramic plate and the cooled ground plate is below 1 K/W in vacuum. Allowing an excess temperature of 100 K, at least 100 W of dissipated power can be tolerated on each chopper plate. This value is amply sufficient for the heat load expected for the most demanding linac operation scenario.

4.5 High voltage

At nominal operation, the electric field at the center of the aperture should be 40 kV/m. With a coverage factor of the order of 0.8 and some losses on the plates voltages to ground of roughly ±600 V will be necessary. A static test voltage was chosen for two reasons.

- Due to the long required burst with low droop the pulser low frequency cut-off has to start practically at DC, that is, roughly at 100 kHz [23]. Since the Kilpatrick limit increases with frequency, measuring at DC should give a pessimistic value for the break-down field.
- A DC high voltage generator is much easier to find and operate than an RF source of sufficient power.

The high voltage generator was connected at one end of the chopper plate and the second port left open. While the voltage was slowly increased the current was monitored with an Amperemeter sensitive down to 1 μA. The vacuum pressure at the beginning of the tests was $3.1 \cdot 10^{-8}$ mbar.
When the chopper plates are set to a positive polarity with respect to ground, voltages up to 1.5 kV could be applied without measurable leakage currents. Starting at about 2 kV short current bursts were observed which disappeared after a few seconds due to apparent conditioning of the emitting surfaces. A stable situation with leakage currents below the level of sensitivity at 2.5 kV was reached without problems.
For negative polarity field emission was found starting at about 1 kV, with currents of the order of 10 μA and the vacuum pressure temporarily rising up to $1 \cdot 10^{-7}$ mbar. After short conditioning a stable situation with currents below measurement sensitivity was soon reached at 2 kV, however going beyond 2.4 kV appeared difficult due to persistent "leakage" currents above 10 μA.
To summarize the results, a static voltage of more than 2 kV to ground in both polarities could be put on the single chopper plate under vacuum. Since the distance between two plates is rather large (20 mm) and there are not sharp edges on the meander lines facing each other similar results should are expected with both plates installed. Therefore the chopper should stand a static voltage of at least 4 kV between the two plates. For pulsed operation this limit should be still higher. The lower threshold for negative polarity is apparently due to electron emission from sharp edges on the meander line or its feed lines. The transition region between the coaxial feed line and the meander is suspected to be the limiting factor due to the rather thin conductor band and its small distance to ground (< 2 mm).

Conclusion

The deflecting structure for the SPL chopper has been successfully designed, prototyped and tested. A slow-wave structure build as a meander line printed on a ceramic substrate was chosen as the most promising candidate for the chopper plates. A number of technological hurdles related to the printing of the meander line had to be overcome. The structure is not very sensitive to radiation, it can stand the required heat load and the vacuum pressure is well within specifications. RF and high voltage tests also gave very satisfying results.

Remaining jobs

The next planned steps are

- Procurement the remaining ceramic plates
- Installation of all four plates in the two tanks
- Full lab testing of the two tanks, including RF, vacuum & leak tightness, high voltage and possibly heat transfer
- Test with a pulse generator
- Beam test with static voltage and with pulser

Acknowledgements

We would like to thank the AB-RF workshops for assembling the tank, F. Wurster and M. Nagata from Kyocera for fruitful cooperation in development and implementation of the technologies for printing the meander structure and J. Borburgh for assistance with the heat transfer measurements. Thanks to R. Garoby and T. Linnecar for support.
We acknowledge the support of the European Community Research Infrastructure Activity under the FP6 "Structuring the European Research Area" programme (CARE, contract number RII3-CT-2003-506395).

Bibliography

[1] Gerigk, F. (ed), *Conceptual design of the SPL II: A high-power superconducting H^- linac at CERN*, CERN-2006-006, Geneva (2006)

[2] Meinke, H. and Gundlach, F. W., *Taschenbuch der Hochfrequenztechnik*, Dritte Auflage, Springer-Verlag, Berlin (1968), in German

[3] Meinke, H. and Gundlach, F. W., *Taschenbuch der Hochfrequenztechnik*, Vierte Auflage, Springer-Verlag, Berlin (1986), in German

[4] Bruno, L., Lombardi, A., Magistris, M., Silari, M., *The beam absorbers of the 3 MeV H^- Test Facility at CERN*, CARE-Note-2006-004-HIPPI, CERN, Geneva (2006)

[5] Sullivan, A. H., *A Guide to Radiation and Radioactivity Levels near High Energy Particle Accelerators*, Nuclear technology publishing, Ashford (1992)

[6] Kilpatrick, W. D., *Criterion for vacuum sparking designed to include both RF and DC*, The Review of Scientific Instruments, Vol. 28, No. 10, (1957)

[7] Magistris, M., *Private Communication* (2006)

[8] Schönbacher, H., Stolarz-Izcka, A., *Compilation of radiation damage test data: materials used around high-energy accelerators*, CERN-82-10, Geneva (2006)

[9] Zeller, A., *Inorganic Insulation for Use in High Radiation Environments*, http://at-hhh-amt.web.cern.ch/AT-HHH-AMT/Presentations/AZeller.pdf

[10] Clarke-Gayther, M., *RAL slow-wave electrode designs for a 3 MeV MEBT fast chopper*,
http://www.fz-juelich.de/ikp/hippi/autumn2006/HIPPI06_CGayther2.pdf

[11] Clarke-Gayther, M., *A fast beam chopper for next generation high power proton drivers*,
CARE Conf-04-008-HIPPI, Proceedings of the EPAC04, Lucerne (2004)

[12] Caspers, F., Mostacci, A., Kurennoy, S., *Fast Chopper Structure for the CERN Superconducting Proton Linac*, Proceedings of the EPAC02, Paris (2002)

[13] Caspers, F., *Impedance Determination*, in: *Handbook of Accelerator Physics and Engineering*, World Scientific (1998)

[14] Kurennoy, S.S., Power, J.F., *Development of meander line current structure for SNS 2.5-MeV beam chopper*, Proceedings of the EPAC, Vienna, (2000)

[15] Kurennoy, S. S., Power, J. F., *Meander-Line Current Structure Development for SNS Fast Chopper*, Proceedings of the EPAC 2000, Vienna (2000)

[16] Hoffmann, R.K., *Integrierte Mikrowellenschaltungen*, Springer, Berlin (1983), in German

[17] Adam, J., *Neues von der Strombelastbarkeit von Leiterbahnen*, GMM-Fachbericht 44 (2004), in German

[18] Flomerics Ltd, http://www.flomerics.de, *Private Communication* (2005)

[19] PMB, *Traversee* 50 Ω *Type N mod.*, Drawing number 1751.00.00 (2002)

[20] Caburn MDC Europe Ltd, http://www.caburn.co.uk/, *Coaxial feedthrough catalogue, part number 924200* (2006)

[21] Pardo, R. C., Bogaty, J. M., Clifft, B. E., *First Tests of a Traveling-Wave Chopper for the ATLAS Positive Ion Linac*, Proceedings of the Linac '98, Chicago (1998)

[22] Novikov-Borodin, A. V.; Kutuzov, V. A., Ostroumov, P., *A Fast Chopper for Intensity Adjustment of Heavy-Ion Beams*, Proceedings of the PAC 2005, Knowville (1998)

[23] Paoluzzi, M., *Status of the CERN Chopper Driver and the Solid State Alternative*, CERN-AB-Note-2005-031 RF, Geneva (2005)

[24] Paoluzzi, M., *Private communication* (2006)

[25] Kroyer, T., Paoluzzi, M., *CERN chopper and driver status report*, http://www.fz-juelich.de/ikp/hippi/autumn2006/HIPPI06_Kroyer_report.pdf (2006)

[26] Naterer, G. F., *Heat transfer in Single and Multiphase Systems*, CRC Press, Boca Raton (2003)

[27] Lebrun, P., Milner, S., Poncet, A., *Cryogenic design of the stochastic cooling pick-ups for the CERN antiproton collector (ACOL)*, 1985 Cryogenic Engineering Conference and International Cryogenic Materials Conference, Cambridge (1985)

[28] Zinke, H. and Brunswig, H., *Lehrbuch der Hochfrequenztechnik*, Springer-Verlag, Berlin (1973), in German